J Mater Sci (2009) 44:5235–5248
DOI 10.1007/s10853-009-3460-5

FERROELECTRICS

Hypertoroidal moment in complex dipolar structures

S. Prosandeev · L. Bellaiche

Received: 12 March 2009 / Accepted: 1 April 2009 / Published online: 24 April 2009

Abstract The very recent use of atomistic simulations to investigate low-dimensional ferroelectrics and ferromagnets has led to the discovery of a new order parameter that is associated with the formation and evolution of many complex dipolar structures (such as onion and flower states or double vortices). Such new order parameter has been named as the hypertoidal moment, involves a double cross product of the local dipoles with the vectors locating their positions, and provides a measure of subtle microscopic features. Here, the recent studies devoted to the discovery of such order parameter and how to control it in *zero-dimensional* systems are reviewed. We also give additional information, such as the symmetry, conjugate field and associated susceptibility of the electric and magnetic hypertoidal moments. A discussion about the existence of the hypertoidal moment and its evolution as a function of temperature and applied field, as well as its possible multivalues, is also provided for complex states (such as nanostripes and nanobubbles) in *periodic* dipolar systems.

Introduction

The need of miniaturizing devices and the quest of finding original phenomena have led to a flurry of research in the field of low-dimensional ferroelectric and magnetic systems in the last 10 years. As a result, interesting and exciting discoveries of fundamental and technological importance have been made. In particular, novel complex dipolar states have been found to occur and to possess new order parameters (in addition to, or even in replacement of, the polarization/magnetization in low-dimensional ferroelectrics/ferromagnets). For instance, the toroidal moment, which involves the cross product of the local dipoles with their positions [1], is the sole order parameter associated with the (single) vortex states that have been discovered in zero-dimensional ferroelectrics [2] and ferromagnets [3] 5 and 8 years ago, respectively. Another example is the very recent prediction [4], through the use of atomistic simulations, of another multipole that acts as an order parameter of various, complex dipolar states in zero-dimensional ferroelectrics and ferromagnets. Such new multipole has been named as the hypertoroidal moment in Ref. [4], involves a *double cross* product of the local dipoles with the vectors locating their positions. It provides a measure of some subtle microscopic features, such as the helicity of the two domains inherent to onion states, the curvature of the dipolar pattern in flower states or characteristics of set of vortices with opposite chirality (e.g., distance between vortices' centers and/or magnitude of their local dipoles). Interestingly, Ref. [5] further indicated that one can control such new order parameter—through the application of some fields in some peculiar zero-dimensional systems (e.g., hysterons or elongated nanodots). Such possible control may be put in use to design a new generation of, e.g., efficient memory nanodevices.

The aim of this manuscript is to review the studies of Refs. [4, 5], as well as, to provide additional information related to the electric and magnetic hypertoroidal moments. This article is organized as follows: section Hypertoroidal moment: definition, symmetry, conjugate fields, and corresponding susceptibility provides the definition of these

S. Prosandeev (✉) · L. Bellaiche
Physics Department, University of Arkansas, Fayetteville, AR 72701, USA
e-mail: sprossan@uark.edu

S. Prosandeev
Southern Federal University, 344007 Rostov na Donu, Russia

hypertoroidal moments, and indicates its symmetries, conjugate fields, and associated susceptibilities. Section Hypertoroidal moment in zero-dimensional dipolar systems mostly reviews the two studies reporting the discovery of the existence and control of these hypertoroidal moments in zero-dimensional ferromagnets and ferroelectrics [4, 5], and gives information about the numerical methods used there. Section Hypertoroidal moment in two-dimensional dipolar systems is devoted to hypertoroidal moments in periodic (e.g., 2D) systems. In particular, section Hypertoroidal moment in two-dimensional dipolar systems reveals that such hypertoroidal moments can be used as a fingerprint of unusual evolutions of the dipolar configurations and that, unlike in zero-dimensional systems, exhibit different possible values depending on the choice made for the supercell mimicking these periodic systems. Finally, section Conclusion concludes this article.

Hypertoroidal moment: definition, symmetry, conjugate fields, and corresponding susceptibility

Definition

In order to better appreciate the origin of the hypertoroidal moment, let us first discuss the definition of the toroidal moment originally given in Refs. [1, 6]

$$T_\alpha = \frac{1}{10V}\int [(\mathbf{r}\cdot\mathbf{j})r_\alpha - 2r^2 j_\alpha]\mathrm{d}^3 r, \tag{1}$$

where α denotes a Cartesian component, V the volume of the investigated system, $\mathbf{r}$ the position vector (with respect to the origin), and $\mathbf{j} = curl\mathbf{p}$ —with $\mathbf{p}$ being the (magnetic or electric) dipole moment. Equation 1 results from a multipole expansion of $\mathbf{j}$ in terms of power of position, and indicates that the toroidal moment is associated with the second order in that expansion. Interestingly, one can prove through the help of integral theorems that Eq. 1 can be rewritten as [1]:

$$\mathbf{T} = \frac{1}{V}\sum_i \mathbf{T}_i = \frac{1}{2V}\sum_i \mathbf{r}_i \times \mathbf{p}_{it}, \tag{2}$$

where

$$\mathbf{T}_i = \frac{1}{2}\mathbf{r}_i \times \mathbf{p}_{it} \tag{3}$$

is the individual toroidal moment associated with the site i (that is located at $\mathbf{r}_i$) and $\mathbf{p}_{it}$ is the *transverse* component of the (electric or magnetic) dipole moment at this site i.

Let us now define $\mathbf{J} = curl\mathbf{T}$ (that is, consider, e.g., systems for which the toroidal moment can be "strongly" space dependent), and introduce a new physical quantity, the hypertoroidal moment, by "simply" replacing $\mathbf{j}$ by $\mathbf{J}$ in Eq. 1:

$$h_\alpha = \frac{1}{10V}\int [(\mathbf{r}\cdot\mathbf{J})r_\alpha - 2r^2 J_\alpha]\mathrm{d}^3 r. \tag{4}$$

The hypertoroidal moment can also be rewritten by substituting in Eq. 2 the *individual* dipole moments by the *individual* toroidal moments. In other words, one can write:

$$\mathbf{h} = \frac{1}{2V}\sum_i \mathbf{r}_i \times \mathbf{T}_{it} = \frac{1}{4V}\sum_i \mathbf{r}_i \times (\mathbf{r}_i \times \mathbf{p}_{it})_t, \tag{5}$$

where $\mathbf{T}_{it}$ is the transverse component of the individual toroidal moment.

Note that we numerically checked (for all the various cases we considered) that the transverse component of the individual dipoles and individual toroidal moment can be well approximated by:

$$\mathbf{p}_{it} \approx \mathbf{p}_i - \langle\mathbf{p}\rangle, \tag{6}$$

$$\mathbf{T}_{it} \approx \mathbf{T}_i - \langle\mathbf{T}\rangle, \tag{7}$$

where $\langle\mathbf{p}\rangle$ and $\langle\mathbf{T}\rangle$ are the average over all sites of the individual dipole and toroidal moments, respectively. Interestingly, such approximations make $\mathbf{T}$ and $\mathbf{h}$ independent on the choice of the origin for the $\mathbf{r}_i$ vectors in any *zero-dimensional* systems (i.e., for systems that are finite in any Cartesian direction). Such approximations make also $\mathbf{T}$ and $\mathbf{h}$ independent on the choice of the origin for the $\mathbf{r}_i$ vectors for a given (periodic) supercell in any *one-dimensional*, *two-dimensional*, and *three-dimensional* systems, but, as we will see later in subsection Multivaluedness of the hypertoroidal moment in thin films, $\mathbf{T}$ and $\mathbf{h}$ do depend on the choice of the supercell made for mimicking systems that are periodic in one, two, or three directions.

Symmetry

Note that Eq. 5 allows us to determine the symmetry of the *magnetic* hypertoroidal moment, $\mathbf{h}_\mathrm{m}$ (i.e., for which the involved dipoles are magnetic), and of the *electric* hypertoroidal moment, $\mathbf{h}_\mathrm{e}$ (for which the involved dipoles are electric). Here, we follow the Ascher notations [7], and indicate in Table 1 how $\mathbf{h}_m$ and $\mathbf{h}_\mathrm{e}$ transform under space and time inversion (Table 1 also reports the already known transformation of the magnetization $\mathbf{M}$, electrical

Table 1 Transformation of different order parameters under space and time inversion

	$\mathbf{M}$	$\mathbf{P}$	$\mathbf{T}_\mathrm{m}$	$\mathbf{T}_\mathrm{e}$	$\mathbf{h}_\mathrm{m}$	$\mathbf{h}_\mathrm{e}$
$\mathbf{r} \to -\mathbf{r}$	+	−	−	+	+	−
$t \to -t$	−	+	−	+	−	+

$\mathbf{M}$, $\mathbf{P}$, $\mathbf{T}_\mathrm{m}$, $\mathbf{T}_\mathrm{e}$, $\mathbf{h}_\mathrm{m}$, and $\mathbf{h}_\mathrm{e}$ represent the magnetization, polarization, magnetic toroidal moment, electric toroidal moment, magnetic hypertoroidal moment and electric hypertoroidal moment, respectively

polarization $\mathbf{P}$, magnetic toroidal moment $\mathbf{T}_m$, and electric toroidal moment $\mathbf{T}_e$, for the sake of completeness [1, 7]). One can notice that the magnetic hypertoroidal moment transforms as the magnetization: they are both axial vectors (since they are invariant under space inversion) and both change their sign under time inversion. Similarly, $\mathbf{h}_e$ transforms as the polarization, and is thus a polar vector (since it changes its sign under space inversion) in addition to be invariant under time inversion.

Knowing such symmetries is important to, e.g., determine which physical quantities can interact with which order parameters or how a combination of different order parameters can influence or even induce another order parameter. For instance, it is interesting to realize that the cross product between $\mathbf{T}_m$ and $\mathbf{h}_m$ transforms (under space and time reversal) in the same way than the electrical polarization. This implies that a material possessing a non-zero magnetic toroidal moment and a non-zero magnetic hypertoroidal moment, with $\mathbf{T}_m$ and $\mathbf{h}_m$ being neither parallel nor antiparallel to other, can be an improper *ferroelectric* (i.e., it can exhibit an electric polarization induced by the combination of $\mathbf{T}_m$ and $\mathbf{h}_m$,) in the same manner than a cycloidal spin structure can generate a polarization [8] through the Dzyaloshinskii–Moriya model [9, 10].

Conjugate fields

Let us now determine what are the conjugated fields of $\mathbf{h}_m$ and $\mathbf{h}_e$. For that, it is useful to recall that the fields conjugated to $\mathbf{T}_m$ and $\mathbf{T}_e$ have already been derived in the literature [11] and are $\nabla \times \mathbf{B}$ and $\nabla \times \mathbf{E}$, respectively. In other words, the field conjugate to a magnetic (respectively, electric) toroidal moment is the curl of the field that is conjugate to the magnetization (respectively, polarization). Since the passage from individual dipoles to the toroidal moment is similar to the passage from individual toroidal moments to the hypertoroidal moment (they both involve cross products with vectors locating the sites), one can deduce that the conjugated field $\mathbf{F}_m$ of $\mathbf{h}_m$ is

$$\mathbf{F}_m = \nabla \times (\nabla \times \mathbf{B}) \tag{8}$$

and that the conjugated field $\mathbf{F}_e$ of $\mathbf{h}_e$ is

$$\mathbf{F}_e = \nabla \times (\nabla \times \mathbf{E}). \tag{9}$$

Non-zero values of the conjugate fields of $\mathbf{h}_m$ and $\mathbf{h}_e$ thus require the creation of highly inhomogeneus-in-space magnetic or electric fields, respectively, such as $\frac{1}{2}\mathbf{r} \times (\omega \times \mathbf{r})$ where ω is a constant vector. Note that we numerically checked, when investigating double vortices (for which the sole order parameter is the hypertoroidal moment, see subsections Magnetic hysterons and Ferroelectric nanodots), that such field (for which *curlcurl* is simply equal to ω at any point in space) can indeed affect and even control hypertoroidal moment.

Hypertoroidal susceptibility

The change of the magnetic or electric hypertoroidal moment with respect to its conjugate field is a physical quantity that we can denote as the hypertoroidal susceptibility, based on the analogy with the magnetic (respectively, dielectric) susceptibility that quantifies the response of the magnetization (respectively, polarization) to a magnetic (respectively, electric field). In other words, one can define the magnetic hypertoroidal susceptibility, $\chi^{(hm)}$, and the electric hypertoroidal susceptibility, $\chi^{(he)}$, as:

$$\chi^{(hm)}_{\alpha\beta} = \mu_0 \frac{\mathrm{d}h_{m,\alpha}}{\mathrm{d}[\nabla \times (\nabla \times \mathbf{B})]_\beta} \tag{10}$$

$$\chi^{(he)}_{\alpha\beta} = \frac{1}{\varepsilon_0} \frac{\mathrm{d}h_{e,\alpha}}{\mathrm{d}[\nabla \times (\nabla \times \mathbf{E})]_\beta}, \tag{11}$$

where α and β are Cartesian indices, μ_0 the vacuum permeability, and ε_0 the vacuum permittivity.

Interestingly, it is straightforward to prove that the hypertoroidal susceptibilities can be practically determined by computing correlation functions of the considered system *under no field*. Such useful feature originates from the fluctuation-dissipation theorem [12], is similar to the fact that the dielectric susceptibility is well known to be related to polarization's fluctuations [13], and yields here:

$$\chi^{(hm)}_{\alpha\beta} = \frac{\mu_0 V}{k_B T}\left[\langle h_{m,\alpha} h_{m,\beta}\rangle - \langle h_{m,\alpha}\rangle\langle h_{m,\beta}\rangle\right], \tag{12}$$

$$\chi^{(he)}_{\alpha\beta} = \frac{V}{\varepsilon_0 k_B T}\left[\langle h_{e,\alpha} h_{e,\beta}\rangle - \langle h_{e,\alpha}\rangle\langle h_{e,\beta}\rangle\right], \tag{13}$$

where V is the volume of the system, k_B the Boltzmann constant, T the temperature, and "$\langle\ \rangle$" denotes thermal averages.

Hypertoroidal moment in zero-dimensional dipolar systems

The aim of this section is to mostly review recent articles that reported the discovery of the hypertoroidal moment, and how to control it, in different zero-dimensional systems made of ferromagnets or ferroelectrics [4, 5] (note that we also report additional information in subsections Ferroelectric nanodots and Ferroelectric half-cut rings that were never published before). This discovery occurred through simulations. As a result, it is important to first (briefly) discuss the methods used in these simulations.

Methods

Ferromagnets

For zero-dimensional ferromagnets having characteristic sizes of the order of several hundred, or even thousand, of nanometers (such sizes are needed to obtain complex dipolar configurations [14–16]), the hybrid approach of Ref. [15] that combines both atomistic and continuum features was used. In this scheme, the investigated ferromagnet is divided into equal regions (cells) of b^3 volume and containing several unit cells. The total magnetic moment of any of such region j, $\mathbf{p}_j$, is equal to the sum of the $\mathbf{p}_{i,j}$ local magnetic moments of the magnetic atoms i belonging to that region, assuming that the $\mathbf{p}_{i,j}$ are all identical inside a given region. The total energy of the studied zero-dimensional ferromagnetic structures under a magnetic field, $\mu_0\mathbf{H}$ (with μ_0 being the permeability of vacuum), is given by:

$$E_{\text{magn}} = \frac{1}{2}\sum_{jk\alpha\beta} D_{j\alpha,k\beta} p_{j\alpha} p_{k\beta} - \mu_0 \mathbf{H} \cdot \sum_j \boldsymbol{p}_j + \frac{1}{2} J \sum_{jk\alpha} p_{j\alpha} p_{k\alpha}, \tag{14}$$

where the sums run over the cells j and k and over the Cartesian components α and β. $D_{j\alpha,k\beta}$ is the tensor associated with the long-range magnetic dipole–dipole interactions [15], and the sum over k in the last term only runs over the first nearest neighbors of the cells j. The short-range exchange interaction parameter between the $\boldsymbol{p}_j$'s is estimated from the usual material exchange constant A as $J = Aa/(n^5|\mathbf{p}_{i,j}|^2)$, where a is the material primitive lattice constant and where $n = b/a$ is an integer. The ferromagnetic systems investigated in Refs. [4, 5] were mimicked to be made of Permalloy 80 (i.e., $Ni_{80}Fe_{20}$) by using the parameters [16] $A = 1.3 \times 10^{-6}$ erg/cm, $|\mathbf{p}_{i,j}| = 0.205\mu_B$ (where μ_B is the Bohr magneton) and $a \simeq 3$ Å. E_{magn} was then used to solve the Landau-Lifshitz molecular dynamics equations [17] for all the $\boldsymbol{p}_j$ (note that this hybrid method technically differs from the approaches previously used for low-dimensional ferromagnets [18–20]).

Ferroelectrics

Prosandeev and Bellaiche [4, 5] considered zero-dimensional stress-free ferroelectrics made of $Pb(Zr_{0.4}Ti_{0.}6)O_3$ (PZT), and having {001} Pb–O terminated surfaces. Their total energy is given by:

$$E_{\text{tot}} = E_{\text{mat}}(\{\mathbf{p}_i\}, \{\mathbf{v_i}\}, \hat{\eta}, \{\sigma_i\}) + \frac{\beta}{2}\sum_i \langle \mathbf{E}_{\text{dep}} \rangle \cdot \mathbf{p}_i + E_{\text{surf}}(\{\mathbf{p}_i\}, \{\mathbf{v}_i\}), \tag{15}$$

where $\mathbf{p}_i$ is the electrical dipole moment at the site i of the supercell and $\mathbf{v}_i$ is a dimensionless vector related to the inhomogeneous strain around this site [21, 22], while $\hat{\eta}$ is the homogeneous strain tensor. $\{\sigma_i\}$ characterizes the alloy configuration [23, 24] that is presently randomly chosen, in order to mimic a disordered system. The expression and first-principles-derived parameters of E_{mat}, the intrinsic alloy effective Hamiltonian energy, are those given in Refs. [23, 24] for PZT *bulk*, except for the dipole–dipole interactions for which the analytical expressions derived in Refs. [25–27] were used for the investigated zero-dimensional PZT systems under *ideal open-circuit conditions* (OC). Such electrical boundary conditions naturally lead to the existence of a maximum depolarizing field (denoted by $\langle \mathbf{E}_{\text{dep}} \rangle$ and determined from the atomistic approach of Refs. [26, 27]) inside the system for a non-vanishing polarization. The second term of Eq. 15 mimics a screening of $\langle \mathbf{E}_{\text{dep}} \rangle$ via the β parameter. More precisely, $\beta = 0$ corresponds to ideal OC conditions, while an increase in β lowers the magnitude of the resulting depolarizing field, and $\beta = 1$ corresponds to ideal short-circuit (SC) conditions for which the depolarizing field has vanished. The third term of Eq. 15 , E_{surf}, mimics how the existence of free surfaces affects the dipoles and strains near them [28, 29]. Its analytical expression is indicated in Ref. [29], with its parameters having been determined from a first-principles computation on a PZT slab surrounded by vacuum. The total energy of Eq. 15 was used in Monte Carlo (MC) simulations [30] or molecular dynamics [31].

Magnetic hypertoroidal moment in zero-dimensional ferromagnets

Let us now discuss the discovery of the *magnetic* hypertoroidal moment, and related effects, in zero-dimensional ferromagnets.

Asymmetric ferromagnetic rings

An asymmetric ferromagnetic ring made of Permalloy 80 was investigated in Ref. [4], using the method described in subsection Methods: Ferromagnets, in order to discover the existence of the magnetic hypertoroidal moment. Practically, the studied system has a height $h \simeq 250$ nm, and an internal and external radii about the z-axis (that lies along the [001] direction) equal to $r \simeq 417$ nm and $L \simeq 1056$ nm, respectively. This ring was made asymmetric in shape by shifting along the x-axis (that lies along the [100] direction) the center of the internal circle in any (001) plane from the center of the external circle by $S \simeq 167$ nm, as schematized in Fig. 1.

Figure 2 displays the resulting $h_{m,y}$ as a function of $\mu_0 H_y$, at a simulated temperature of $\simeq 100$ K. $\mu_0 H_y$ is the y-component of the ac magnetic field that was solely applied along the y-axis, and was allowed to vary in time

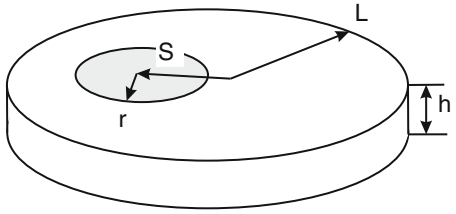

Fig. 1 Schematization of the asymmetrical ring

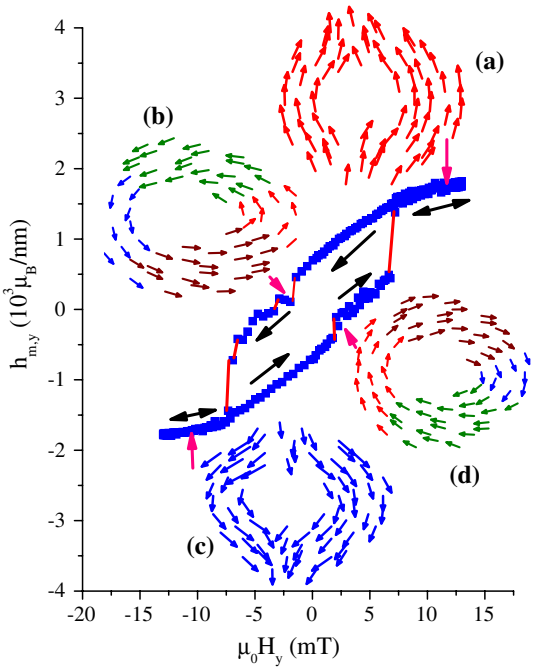

Fig. 2 Predicted hysteresis loop of the magnetic hypertoroidal moment in an asymmetric ferromagnetic ring at 100 K, as a function of the applied ac magnetic field. The insets show the dipolar configurations corresponding to four important states involved in this loop. The *thick arrows* show the direction of the loop

between −10 and +10 mT with a 0.6-MHz frequency. $h_{m,y}$ is the *y*- (and sole) component of the magnetic hypertoroidal moment. Figure 2 indicates that $\mathbf{h}_{\mathrm{m}}$ can be finite and can be considered as an order parameter to represent the complex states, and their evolution, occurring in this ferromagnetic ring under an homogeneous-in-space magnetic field. Moreover, the insets of Fig. 2 provide a snapshot of the dipole arrangement in the four important states predicted by our simulations. These states are: state (a) which is an "onion" state that occurs for the largest positive values of H_y and that exhibits the largest *positive* values for $h_{m,y}$. Interestingly, $h_{m,y}$ is non-zero for an onion state because it provides a measure of the magnitude of the helicity of the two domains inherent to onion states (these two domains have semicircular magnetizations of opposite helicity [32]); state (b) which is a vortex state characterized by a vanishing $h_{m,y}$; state (c) that is another onion state that differs from state (a) by the sign of its $h_{m,y}$; and state (d) that is a vortex state that differs from state (b) by adopting an opposite chirality. Simulations of Ref. [4] further found that the pure onion states (a) or (c) "deform" themselves under the influence of the homogeneous-in-space magnetic field before transforming into the pure vortex states (b) or (d). This deformation mostly consist in pushing the wall between the two kinds of magnetized domains forming the onion state toward the thinner part of the asymmetric ring (i.e., toward the left side of the inner circle), as consistent with Refs. [14, 33]. This deformation leads to a decrease of the magnitude of $h_{m,y}$, as indicated by Fig. 2.

It is also important to realize that $\mathbf{h}_m$ is not the only order parameter of an onion state since such latter state also possesses a non-zero magnetization [4], as it can be guessed from some insets of Fig. 2 (note that, on the other hand, the vortex state has a single order parameter, that is the toroidal moment). Such feature has led the authors of Ref. [4] to look for another complex magnetic state for which the *sole* order parameter is the magnetic hypertoroidal moment, and to wonder how such sole order parameter can be controlled. As we will see below, the double magnetic vortex structure is one structure for which the magnetic hypertoroidal moment is the single order parameter and such moment can be controlled by applying an homogeneous-in-space magnetic field in hysterons made of ferromagnets.

Magnetic hysterons

Prosandeev and Bellaiche [5] studied the ferromagnetic systems schematized in Fig. 3a. They consist of two identical disks of radius *R* merged together, with *w* and *L* representing the thickness of the system and half of the distance between the centers of the two disks, respectively (*L* and *w*

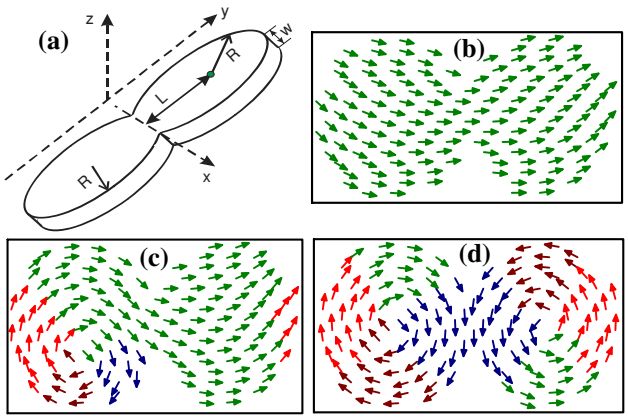

Fig. 3 The geometry of hysterons (**a**) and three different dipole patterns (**b–d**) corresponding to different sizes of magnetic hysterons—**b** small size, **c** intermediate size, and **d** larger size

define the y- and z-axis, respectively). Such low-dimensional structures are called hysterons [34, 35] and have been fabricated in Ref. [34]. To study them, the hybrid approach described in subsection Methods: Ferromagnets was applied again to hysterons made of Permalloy 80.

Figure 3b–d displays the predicted different possible ground-states of an hysteron, depending on the characteristic sizes. For relatively small sizes and when no magnetic field is applied, the ground state of the investigated hysteron is magnetized along the long-axis (see Fig. 3b). When increasing the characteristic sizes, the dipole pattern evolves into the peculiar state that has been discovered in Refs. [32, 33], and that exhibits a dipole vortex in only one of the two disks while the other disk still possesses a magnetized configuration (see Fig. 3c). Finally, when further increasing sizes, the double vortex state appears, as displayed in Fig. 3d, when $R \simeq 1349$ nm, $L \simeq 1178$ nm, and $w \simeq 333$ nm. Such double vortex state has been observed in ferromagnetic hysterons made of permalloys [34] and in other low-dimensional magnets [14, 36, 37]. Interestingly, it was numerically found that the *sole* order parameter of these double vortex structures is the hypertoroidal moment, since such structures do not possess any magnetization or any magnetic toroidal moment (because the two vortices have opposite chiralities) [4, 5].

Prosandeev and Bellaiche [5] further investigated the response of a double vortex to an ac magnetic field applied along the (short) x-axis. Figure 4 shows the (sole) x-Cartesian components of the magnetic hypertoroidal moment, $h_{m,x}$, as a function of H_x/H_m, at a temperature of $\simeq 100$ K for the system adopting the ground-state of Fig. 3d. $\mu_0 H_x$ is the Cartesian component of the magnetic field, which sinusoidally varies in time between $-\mu_0 H_m$ and $+\mu_0 H_m$ (with $\mu_0 H_m = 40$ mT while the field frequency is 0.15 MHz, which is below the resonant frequencies to be in the quasi-adiabatic regime. Such resonant

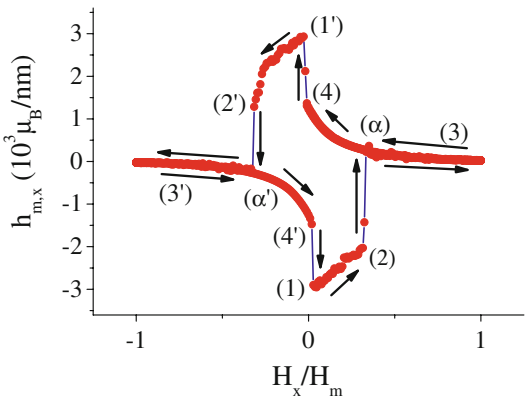

Fig. 4 The dependence of the magnetic hypertoroidal moment in a magnetic hysteron on the ac magnetic field. The *arrows* show the direction of the loop

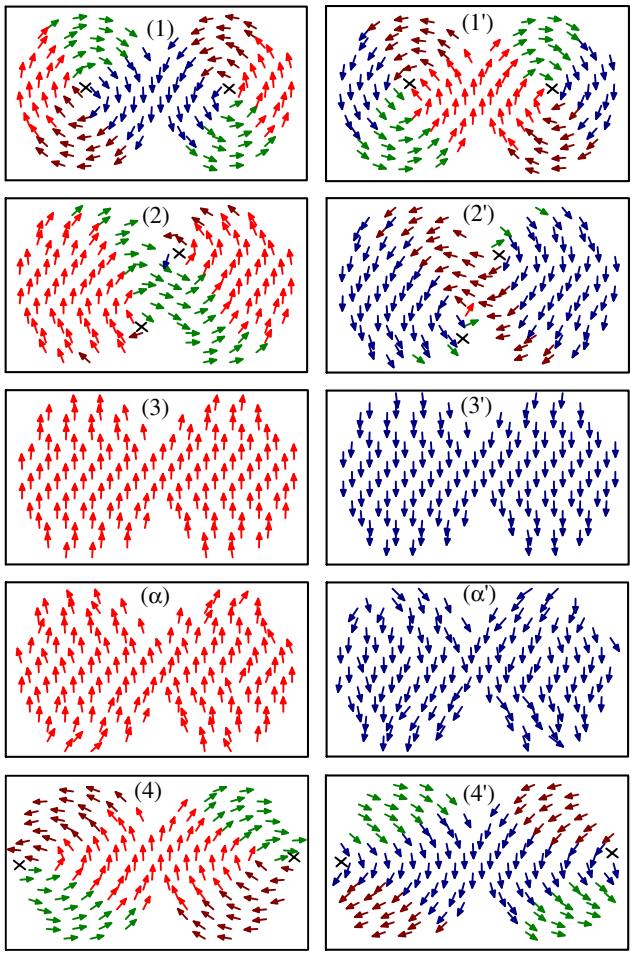

Fig. 5 The important states involved in the hysteresis loop shown in Fig. 4

frequencies are around 10 GHz in mesoscale ferromagnets [38]). Figure 5 provides snapshots of ten important states occurring during these loops. State (1) happens when $H_x = 0$, and is the double vortex state of Fig. 3d. It is therefore associated with a strongly *negative* $h_{m,x}$ (because the vortex centered on the right disk is rotating counterclockwise while the vortex centered on the left disk is rotating clockwise). When $\mu_0 H_x$ slightly increases, the centers of the two vortices move toward each other along the y-axis to create a magnetization along the x-axis and to reduce the magnitude of $h_{m,x}$ through the enlargement of the "up" domains located at the extreme two sides of the hysteron. When these two centers become separated by a critical distance of about 2 ($R-L$), they further move along *different* directions: one center now moves toward the V-shaped junction of the two disks, whereas the other vortex center moves toward the Λ-shaped junction, to prevent the system from possessing too many dipoles having opposite directions within a small distance. Such configuration forms State (2), and was named the "tilde" state in Ref. [5] because of the resemblance between the

shape formed by some lines of dipoles and the tilde character. When further increasing $\mu_0 H_x$, vortices abruptly disappear in favor of State (α), that can be classified as a double onion state since each disk exhibits a configuration that bears resemblance with a (single) onion state [3, 14, 39]. When further increasing $\mu_0 H_x$ up to $+\mu_0 H_m$, State (α) continuously evolves into State (3), by making all the dipoles lying closer to the x-axis. This results in a large positive magnetization along the x-axis and a vanishing $h_{m,x}$. Interestingly, decreasing the field after it reaches its maximum positive value makes State (3) returning to State (α) and then leads to a new configuration, that is State (4). Such latter configuration arises from the simultaneous nucleation of a counterclockwise vortex centered at the extreme left side of the left disk and of a clockwise vortex centered at the extreme right side of the right disk. $h_{m,x}$ is large and *positive* in State (4) because State (α) acts as a seeding state for State (4) and because State (α) has a positive magnetic hypertoroidal moment resulting from its specific dipole pattern's curvature. State (4) was named the χ state in Ref. [5]. When further decreasing the magnitude of the field but still keeping the positive sign for its x-component, the centers of the two vortices of State (4) move toward each other along the y-axis, until the double vortex State ($1'$) forms when the field vanishes. State ($1'$) differs from State (1) by exhibiting a vortex of *opposite* chirality in each of the two disks, as consistent with the strong *positive* hypertoroidal moment in State ($1'$). The evolution of State ($1'$) to States ($2'$), (α'), ($3'$), (α'), ($4'$), and then back to State (1), when the field first becomes negative in sign, then reaches its lowest possible negative value, and finally increases toward zero, is similar to the evolution from State (1) to State ($1'$), through States (2), (α), (3), and (4), described above for the positive fields—since State (i') is deduced from State (i), for i=1, 2, α, 3, or 4, by a mirror symmetry about the (y,z) plane passing through the center of gravity of the hysteron. Figures 4 and 5 thus indicate that the chirality of each opposite vortex forming the double vortex state (or, equivalently, the sign of the magnetic hypertoroidal moment) can be controlled by applying an homogenous magnetic field parallel to the x-axis, through the formation of the tilde, double onion, homogeneous, and χ states. Interestingly, it was further found in Ref. [5] that starting from State (1) and first applying a *negative* field results in the path (1)–($4'$)–(α')–($3'$)–(α')–*and then back to State* (1), before the hysteresis loops of Fig. 4 occurs again. In other words, one can *not* go from State ($3'$) to State ($2'$) under a negative homogeneous field. This is because the system energetically prefers to exhibit the double onion State (α') that is associated with a *negative* $h_{m,x}$ as its ground-state, for a negative magnetic field of large enough magnitude to result in a large negative magnetization, but not too large to also have a non-vanishing hypertoroidal moment. The hysteresis loop of Fig. 4 can thus only occur in a counterclockwise fashion, and the control of the hypertoroidal moment's sign is inherently linked to the curvature of the dipoles in States (α) and (α').

Electric hypertoroidal moment in zero-dimensional ferroelectrics

Let us now focus on the reported discovery of the *electric* hypertoroidal moment, and its possible control, in zero-dimensional ferroelectrics [4, 5].

Ferroelectric nanodots

Prosandeev and Bellaiche [5] also studied a stress-free cubic ferroelectric (PZT) dot of 24 Å lateral size, and *under ideal SC conditions*. The inset of Fig. 6 represents the dipole arrangement in the ground state of such nanodot, which is a flower state—as consistent with Ref. [26]. Such flower state is polarized along the z-direction but also exhibits a significant deviation, with respect to the z-axis, for the direction of some local electric dipole moments. Such deviations, and their associated helical pattern, are typical of flower states. As a result, any flower state in a ferroelectric material should exhibit a non-zero polarization, as well as a finite electric hypertoroidal moment (that should quantify the helicity associated with such deviations)—as numerically confirmed by Fig. 6 that shows the evolution of the electrical toroidal moment versus temperature in this ferroelectric dot. This figure also shows that the flower state forms around $T_c \simeq 1100$ K, and indicates

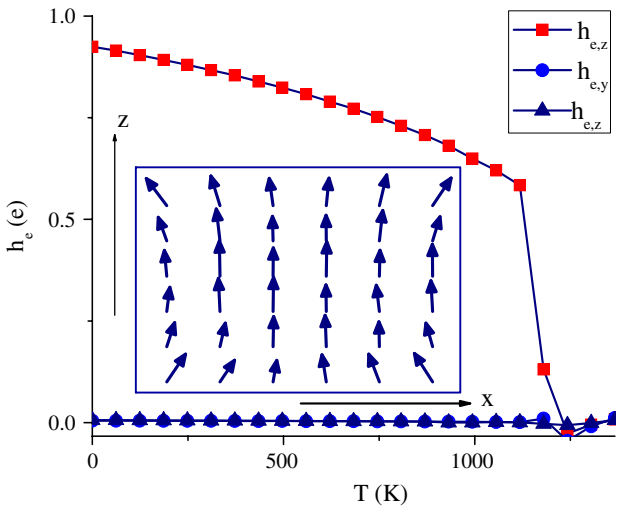

Fig. 6 The dependence of the electric hypertoroidal moment on temperature in a PZT dot under SC electric boundary conditions. The *inset* shows the dipole pattern in the dot obtained at 10 K

that the z-component of the electrical toroidal moment increases when decreasing the temperature below T_c—as a result of the increase in the magnitude of the local dipole moments (note that flower states have also been seen in *magnetic* nanostructures of relatively small size [40], and should thus be associated with a magnetic hypertoroidal moment there).

An elongated 24 Å × 48Å × 96 Å stress-free PZT dot surrounded by vacuum all around it (that is *under ideal OC conditions*) has also been investigated in Ref. [5]. The inset of Fig. 7a shows the resulting dipole pattern in its ground state. As consistent with Refs. [2, 41], this pattern consists of a double vortex, for which we already know that the *sole* order parameter is the electric hypertoroidal moment (by analogy with the fact that the sole order parameter of magnetic double vortices is the magnetic hypertoroidal moment, see subsection Magnetic hysterons). Figure 7a shows that the y-component of the electric hypertoroidal moment, $h_{e,y}$ versus temperature, and simultaneously reports the temperature dependency of the electric hypertoroidal susceptibility in that elongated PZT dot. On can see that (a) $h_{e,y}$ is zero above a critical temperature $T_{crit} \simeq 555$ K; (b) $h_{e,y}$ increases in magnitude when decreasing the temperature below T_{crit} [the two other Cartesian components of $\mathbf{h}_e$ are null for any temperature]; and (c) the electric hypertoroidal susceptibility peaks at T_{crit}. Such features indicate that the double vortex forms at T_{crit} with the centers of these two vortices being aligned along the z-axis (as seen in the inset of Fig. 7a), and that the dipoles inside these two opposite vortices grow larger in magnitude as the temperature is reduced below T_{crit}.

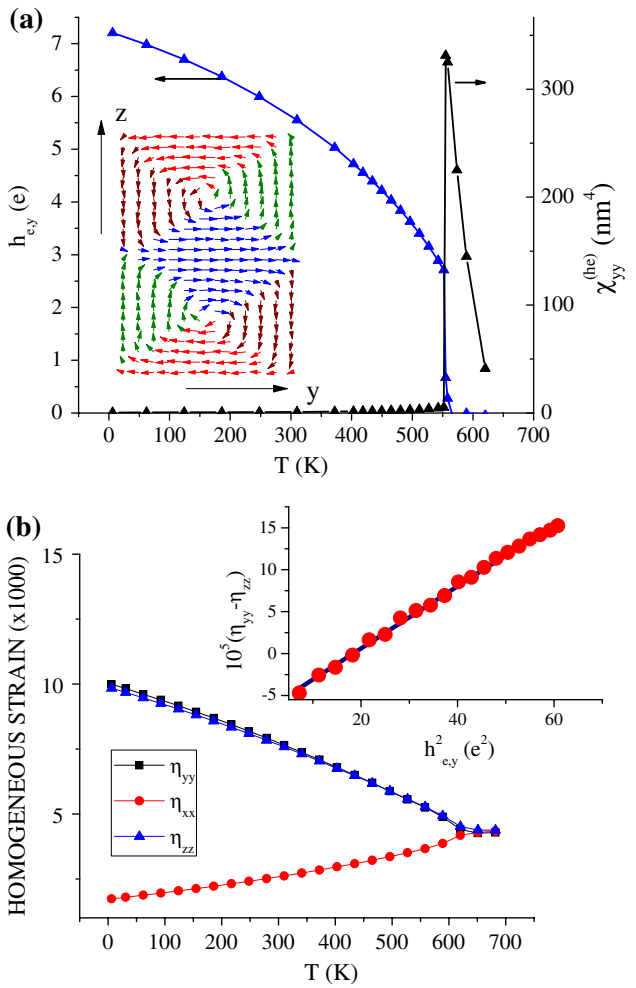

Fig. 7 **a** The dependence of the electric hypertoroidal moment and electric hypertoroidal susceptibility (panel **a**) and of the strain (panel **b**) on temperature in an elongated PZT dot. The *inset* of panel **a** shows the dipole pattern in the dot at 10 K. The *inset* of panel **b** displays the dependence of $\eta_{yy} - \eta_{zz}$ on the square of the hypertoroidal moment

Figure 7b further displays the temperature dependency of the diagonal elements of the homogeneous strain in this PZT elongated dot. One can notice that, below T_{crit}, η_{yy}, and η_{zz} (that are strains in the plane of the vortices, see inset of Fig. 7a) are larger than η_{xx} (which is the strain associated with the direction perpendicular to the vortices). Note also that, below T_{crit}, η_{yy}, and η_{zz} slightly differ, which is consistent with the symmetry of the elongated (along the z-direction) dot. Interestingly, the inset of Fig. 7b reveals that the difference $\eta_{yy}-\eta_{zz}$ is proportional to the square of the hypertoroidal moment for any temperature below T_{crit}. Such findings imply that there is a coupling between strain and hypertoroidal moment. Therefore, any development of Landau-type phenomologies to treat systems having a finite hypertoroidal moment should include an energetic term of the form $\lambda_{l\alpha\beta}\eta_l h_\alpha h_\beta$ where $\lambda_{l\alpha\beta}$ is a tensor, where $l = 1,2,...6$ denotes the use of the Voigt notation for the strain components and where α and β are Cartesian indices. Such coupling is analogous to the piezoelectric effect in polarized systems or to the fact that a strain is induced by a change in the toroidal moment in, e.g., single vortex states [42].

Ferroelectric half-cut rings

Let us also briefly consider systems that also exhibit hypertoroidal moment and that were not considered in Refs. [4, 5].

More precisely, let us first investigate a ring made of PZT, under OC electrical and stress-free mechanical boundary conditions. Practically, this ring is made by cutting a 48 Å × 48 Å × 24 Å hole inside a 96 Å × 96 Å × 24 Å dot. The ground state of such ring is the dipole vortex shown in Fig. 8a. Note that the dipoles in that state always lie parallel to the surface in order to minimize the depolarizing field, and that the sole order parameter of such structure is the electric toroidal moment.

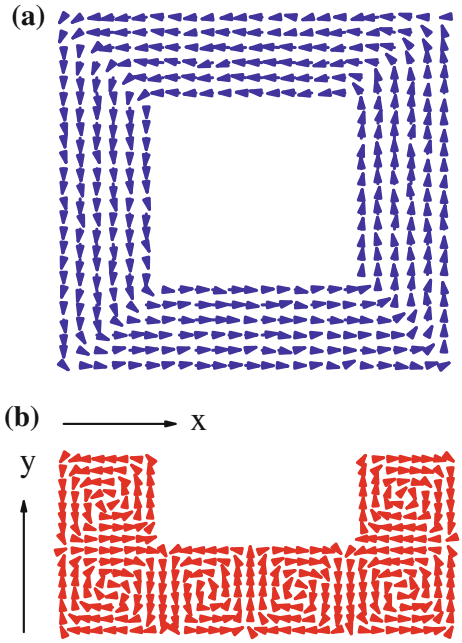

Fig. 8 The dipole pattern in a ring (**a**) and in a half-cut ring (**b**) both made of PZT at 10 K

Let us now cut the ring into two halves and look at its ground state. As one can notice from Fig. 8b, such ground state is no longer a single dipole vortex. It is rather broken into a series of vortices with alternating opposite chiralities, which thus lead to the vanishing of the toroidal moment in favor of the generation of a finite electric hypertoroidal moment that is numerically found to lye along the *y*-direction indicated in Fig. 8.

Ferroelectric hysterons

In order to determine similarities and/or differences between properties of magnetic *versus* ferroelectric systems, Prosandeev and Bellaiche [5] also investigated ferroelectric hysterons—in addition to the magnetic hysterons that have been documented in the subsection Magnetic hysterons. More precisely, the studied ferroelectric hysteron is made of $Pb(Zr_{0.4}Ti_{0.6})O_3$ (PZT), and is under OC electric boundary conditions and stress-free, and its properties were simulated by the effective Hamiltonian approach described in subsection Methods: Ferroelectrics. The characteristic sizes of this hysteron were chosen to be $R = 64$ Å, $L = 12$ Å, and $w = 24$ Å because such small sizes already result in a ground state that is a double vortex. An ac electric field of 10 GHz frequency and with a magnitude of 5×10^8V/m was applied along the (short) *x*-axis of the hysteron (see Fig. 3a for the schematization of an hysteron). It was found that such field is able to control the electric hypertoroidal moment, as analogous to the fact that a magnetic field applied along the *x*-axis of a ferromagnet

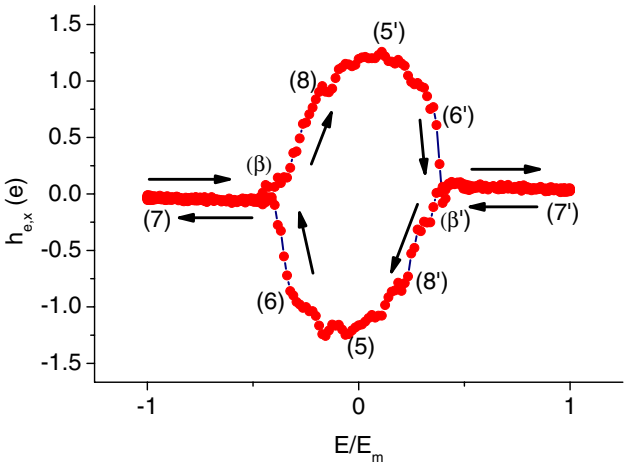

Fig. 9 The dependence of the electric hypertoroidal moment in a ferroelectric hysteron on the ac electric field. The *arrows* show the direction of the loop

hysteron controls the magnetic hypertoroidal moment. However, one major difference was numerically determined between the ferroelectric and magnetic cases: as shown in Fig. 9, the only possible way for the hysteresis loops of the electric hypertoroidal moment-versus-electric field to occur is in a *clockwise* way (while it is in a counterclockwise way for the ferromagnet hysteron, see subsection Magnetic hysterons). To understand the reason behind such difference, Fig. 10 displays the ten important states involved in the control of the electric hypertoroidal moment. The intermediate ferroelectric state denoted as State (β') shown in Fig. 10 has a *negative* electric hypertoroidal moment, whereas the magnetic State (α) depicted in Fig. 5 has a positive magnetic hypertoroidal moment, which explains the opposite path of the hysteresis loops between the ferroelectric and ferromagnet hysterons. Note also that State (β') possesses a small region centered at the junction of the two disks that exhibit dipoles lying in the opposite direction with respect to its polarization, and can therefore be denoted as a ferroelectric bubble state [43]. It is the specific rotation of the dipoles around this small region that yields the negative sign of the hypertoroidal moment. The difference in morphology between such bubble state and the magnetic State (α) originates from the low cost of short-range interactions with respect to depolarizing effects in ferroelectrics, unlike in magnets. Note also that one can notice by comparing Figs. 5 and 10 that some other differences exist between magnetic and ferroelectric hysterons under ac fields. For instance, there is no tilde state in the ferroelectric system, unlike State (2) of the ferromagnetic hysteron. On the other hand, the ferroelectric hysteron exhibits a state that is not seen in the ferromagnetic case. Such state is State (8) for which the centers of the two opposite vortices lie close to each other along the *y*-axis.

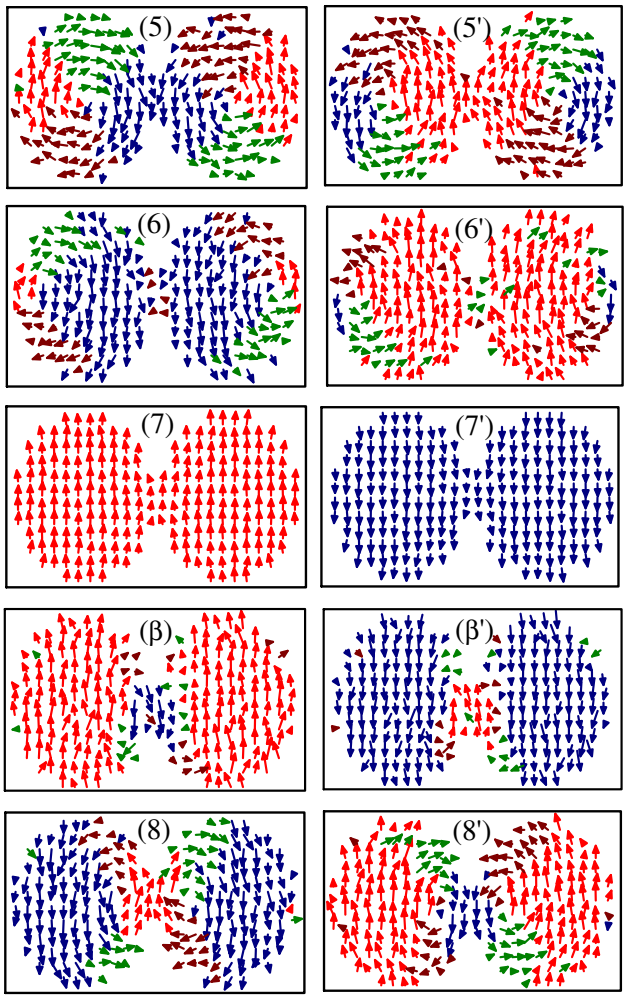

Fig. 10 The important states involved in the hysteresis loop shown in Fig. 9

Hypertoroidal moment in two-dimensional dipolar systems

So far, we focused on hypertoroidal moments in *zero-dimensional* dipolar systems. The aim of this section is to reveal that the hypertoroidal moments can also exist in dipolar systems with higher dimensions (e.g., wires, films, and bulks made of ferromagnets or ferroelectrics), but that the magnitude and even sign of such moments depend on the (periodic) supercell chosen to represent such latter systems. Here, in order to demonstrate such points, it is enough to solely focus on an ultrathin film made of $Pb(Zr_{0.4}Ti_{0.6})O_3$, and having {001} Pb–O terminated surface.

Method for simulating ferroelectric thin films

This PZT thin film is mimicked to be epitaxially grown on a substrate, to have a thickness of 20 Å and to be surrounded by vacuum above it—which implies that it is also under ideal OC electrical boundary condition. It is mimicked by a 16 × 16 × 5 supercell, that is repeated periodically along the *x*- and *y*-directions (chosen to be along the pseudo-cubic [100] and [010] pseudo-cubic directions, respectively) while being finite along the *z*-direction (chosen to lye along [001]).

The total energy of this film, under an external electric field **E**, is written as:

$$E_{\text{tot}} = E_{\text{mat}}(\{\mathbf{p}_i\},\{\mathbf{v_i}\},\hat{\eta},\{\sigma_i\}) + E_{\text{surf}}(\{\mathbf{p}_i\},\{\mathbf{v}_i\}) - \sum_i \mathbf{E}\cdot\mathbf{p}_i\,, \tag{16}$$

where the only differences with Eq. 15 are: (1) that the dipole–dipole interactions involved in E_{mat} are the ones derived in Refs. [25–27] for the *film* (rather than a zero-dimensional system) under ideal OC conditions; (2) we solely deal here with films that are under ideal OC conditions (i.e., the β coefficient of Eq. 15 is null here); and (3) we also incorporate the effect of an electric field on properties of thin films, which explains the existence of the third term of Eq. 16. Moreover, we wish to mimic here thin films that are epitaxially strained on a substrate with a *compressive* misfit strain of 2.65% magnitude, because such mechanical boundary condition is known to generate periodic nanostripes in PZT films under OC-like conditions [44] (and, as we will see below, such nanostripes yield non-zero electric hypertoroidal moment). For that, we freeze three components of $\hat{\eta}$ (in Voigt notation)—$\eta_6 = 0$, and $\eta_1 = \eta_2 = -0.0265$—while its other three components can relax.

The total energy of Eq. 16 is used in MC simulations [30] that typically first run over 4×10^4 MC sweeps to equilibrate the systems at each temperature. Additional 16×10^4 MC sweeps are then used to obtain averaged statistical quantities. The investigated systems are cooled down from high temperatures (in the paraelectric phase) to 10 K, by small steps, which provides us with an accurate measure of the ground-state configuration.

Temperature evolution of the electric hypertoroidal moment and of the electric hypertoroidal susceptibility in a ferroelectric thin film

Figure 11a, b shows the computed electric hypertoroidal moment and the electric hypertoroidal susceptibility, respectively, as a function of temperature in the studied PZT ultrathin film *under no applied field*. One can notice that, at high temperature, $\mathbf{h}_e$ has zero values and that its *z*-component increases upon cooling, while $\chi_{zz}^{(he)}$ increases approximately in a Curie–Weiss manner when decreasing the temperature. Interestingly, $\chi_{zz}^{(he)}$ exhibits two peaks, that are associated with two different behaviors of the electric

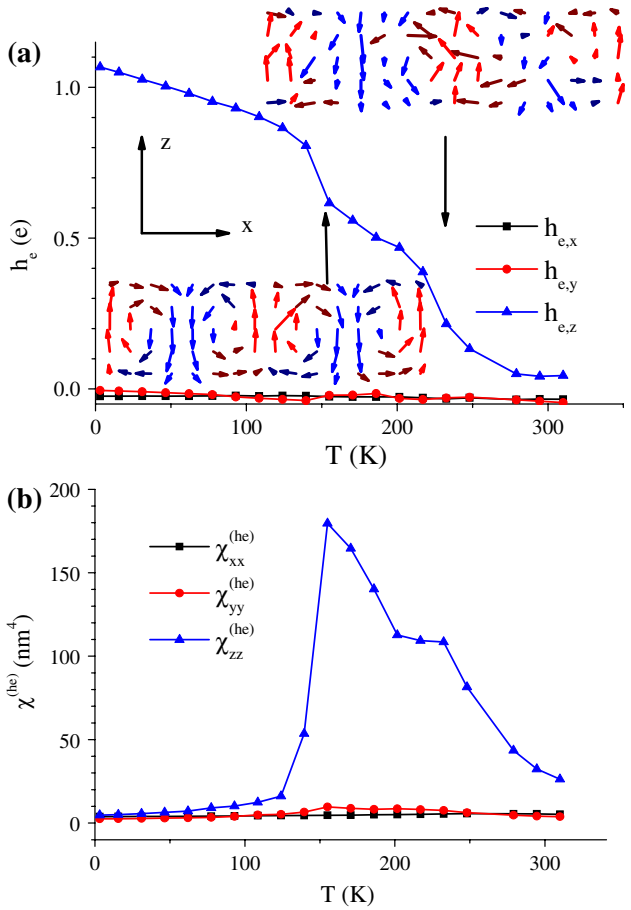

Fig. 11 The temperature dependence of the electric hypertoroidal moment (**a**) and of the electric hypertoroidal susceptibility (**b**) in a thin PZT film. The *insets* of (**a**) represent two different kinds of dipolar configurations

hypertoroidal moment, when further cooling down the system. The first peak occurs around 225 K when the z-component of the electric hypertoroidal moment becomes non-zero. The second peak happens at around 150 K and is associated with an abrupt change of $h_{e,z}$. We numerically found that this first peak corresponds to the appearance of diffused nanostripes made by the z-components of the electric dipoles and repeating themselves along the x-axis (see top inset of Fig. 11a for that configuration), whereas the second peak is generated by the fact that these nanostripes become closed in flux at the top and bottom surfaces of the film for temperature below 150 K (see bottom inset of Fig. 11a for that second configuration). Note that these nanostripes have been experimentally detected [45] and that they do not exhibit any polarization while they are numerically found to also possess a non-zero y-component of the electric toroidal moment (in addition to the z-component of the electric hypertoroidal moment). Figure 11 thus reveals that not only hypertoroidal moments can exist—and act as order parameter—in periodic systems (i.e., in systems with dimensions higher than zero), but also that the behavior of such hypertoroidal moment and of its associated susceptibility can provide information about microscopic changes.

Evolution of the electric hypertoroidal moment as a function of an applied field in a ferroelectric thin film

Let us now check if $\mathbf{h}_e$ can also act as fingerprints for the unusual evolution from nanostripe domains to monodomains, through the formation of nanobubbles, that has been recently predicted to occur in compressively strained ferroelectric films under OC like conditions and under an applied dc electric field [43]. For that, Fig. 12 reports the electric hypertoroidal moment as a function of the E_z magnitude of an electric field **E** oriented along the z-axis for the investigated PZT film at 10 K.

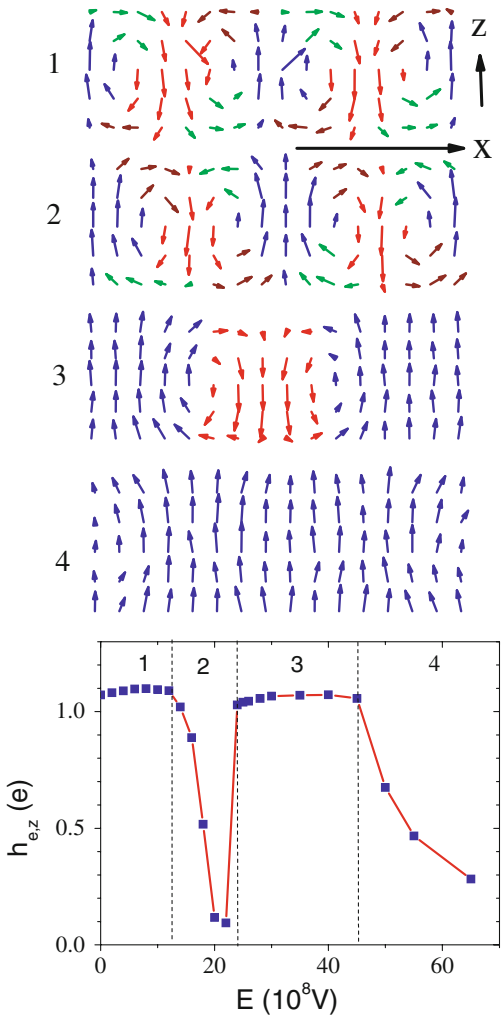

Fig. 12 The dependence of the electric hypertoroidal moment in a PZT thin film on the electric field magnitude. Snapshots of the four important states involved in this dependency are shown in the insets

Interestingly, Fig. 12 reveals that the electric hypertoroidal moment adopts four different behaviors depending on the value of the applied field: at small fields (region 1), there is a relatively large electric hypertoroidal moment (along the z-axis), that is nearly independent of E_z. For larger fields, $h_{e,z}$ sharply decreases with E_z until almost vanishing (region 2). Then, at larger fields, the electric hypertoroidal moment recovers a large value that is mostly independent of E_z (region 3), until significantly and sharply decreasing with E_z (region 4).

The microscopic insights provided by our first-principles-based scheme reveal that region 1 corresponds to the domain walls motion of the stripes mentioned in Ref. [43] and depicted in the top inset of Fig. 12, namely that the "up" domains (i.e., for which the dipoles have a z-component aligned along the applied electric field) grow laterally at the cost of the adjacent "down" (antiparallel) domains—with the overall stripe periodicity remaining unchanged. In region 2, the domain walls' motion has stopped (and the "down" domains have reached their minimal size) and the dipoles "simply" rearrange themselves within the "up" and "down" domains—as also seen in Ref. [43]. Region 3 is associated with the formation of the ferroelectric nanobubbles (that are displayed in one inset of Fig. 12 and which possess dipoles aligned along the $-$z-direction) from the pinching of the "down" domains, and with the field evolution of the morphology and number of these bubbles—as also consistent with Ref. [43]. Finally, in region 4, these bubbles have vanished in favor of the homogeneously-like configuration shown in the bottom inset of Fig. 12, in which all dipoles have a significant component along the direction of the applied electric field but with some dipoles still deviating from the z-direction, which explains the non-zero value of $h_{e,z}$. Further increasing E_z in region 4 reorients such dipoles closer to the z-direction, thus leading to a decrease of $h_{e,z}$.

Figure 12 thus further demonstrates that not only the hypertoroidal moment can characterize complex dipolar structures in periodic systems (note that a polarization also develops in the studied film when increasing the magnitude of the applied field [43]), but also that its behavior can indicate subtle microscopic changes in these structures.

Multivaluedness of the hypertoroidal moment in thin films

Let us now numerically determine if and how the value of the hypertoroidal moment depends on the choice of the supercell used to mimic a periodic system. For that, we decided to compute in Fig. 13a $h_{e,z}$ of the nanostripe domains (under no applied field) depicted in the left inset of Fig. 11—that is the Landau-Lifshitz-type (closed flux) periodic nanostripe domains [46]—as a function of a shift s

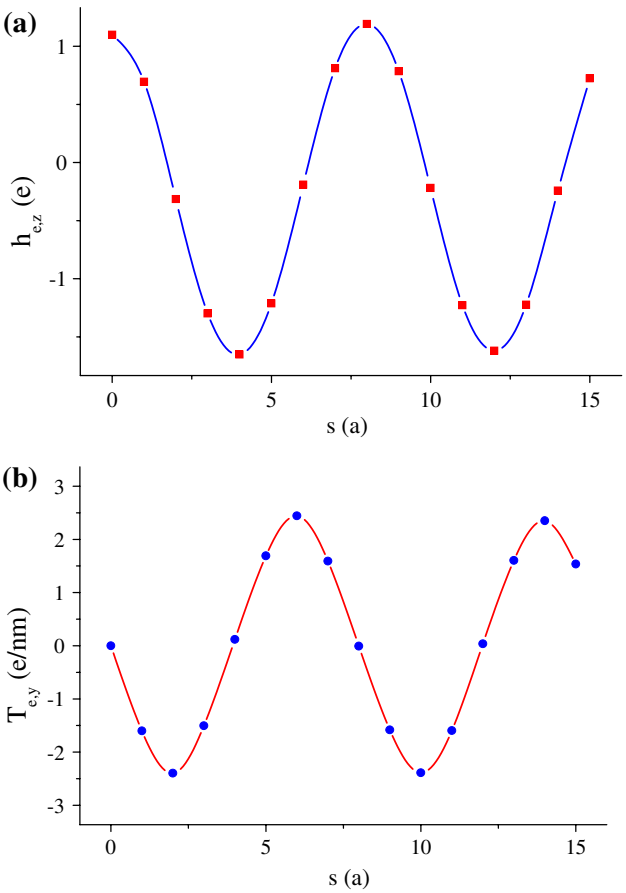

Fig. 13 Dependence of the electric hypertoroidal (**a**) and electric toroidal (**b**) moments on the translation coordinate s (see text) in a thin PZT film

of the 16 × 16 × 5 supercell along the x-axis. $s = 0$ was the choice made for the calculations presented above in the subsections Temperature evolution of the electric hypertoroidal moment and of the electric hypertoroidal susceptibility in a ferroelectric thin film and Evolution of the electric hypertoroidal moment as a function of an applied field in a ferroelectric thin film. On the other hand, for $s = 2$, the origin of the x-axis of the supercell is shifted by two unit cells with respect to the initial supercell and thus coincides with a domain wall. Note that the origin of the x-axis for, e.g., $s = 0$ and $s = 4$ coincides with the core of a up domain and with the core of a down domain, respectively. Figure 13b shows the evolution of the y-component of the electric toroidal moment as a function of the shift s, for the sake of completeness. Figure 13 indicates that the magnitude and even sign of $h_{e,z}$ and $T_{e,y}$ depend on s. In particular, $h_{e,z}$ has a positive maximal (respectively, negative minimal) value for the s's leading to an origin of the x-axis coinciding with the core of an up (respectively, down) domain, while it is the smallest in magnitude for $s = 2$, 6, 10, and 14—that are s for which the origin for the x-axis corresponds to a domain wall. It is

also interesting to notice that the hypertoroidal moment is maximal in magnitude when the toroidal moment is the smallest in magnitude, and vice versa (i.e., the toroidal moment has a maximum magnitude when the hypertoroidal moment is the smallest in magnitude). In fact, Fig. 13 shows that both $h_{e,z}$ and $T_{e,y}$ adopt a sinusoidal dependence with s with a period equal to the period of the nanostripe, and that these two sinusoidal waves have a phase difference of 90 degrees. One can thus decide to define here $h_{e,z}$ and $T_{e,y}$ through their waves characteristics, that are their period, magnitude, phase, and average value.

The fact that the toroidal moment and hypertoroidal moment depend on the choice of the supercell used to represent a periodic system bears resemblance with the fact that the electrical polarization [47] or toroidal moment [48] of a periodic system is *not* uniquely defined and can exhibit different values. Interestingly, such analogy is pushed further when realizing that the *difference* between polarizations (or the difference between toroidal moments) of a given system is known to be physically meaningful (and thus do not depend on the choice of supercell) [49, 50] while we numerically found that the difference between the hypertoroidal moments when the film is within the region 1 indicated in Fig. 12 (e.g., the difference between the hypertoroidal moment, computed for a given s, for a film under an applied field of 10^9 V/m and the hypertoroidal moment, computed for the same s, for a film under no field) is also found to be independent on s.

Conclusion

In summary, we have reviewed the two recent published studies [4, 5] devoted to the electric and magnetic hypertoidal moment in zero-dimensional ferroelectrics and ferromagnets, respectively, through the use of the simulations described in section Methods. We also provided additional information about these hypertoroidal moments. In particular, we emphasized that such new multipole involves a *double cross* product of the local dipoles with the vectors locating their positions, and exists for many complex states, such as the onion, flower, double vortex, nanostripes, and nanobubbles states. In fact, the hypertoroidal moment represents a measure of microscopic features associated with all these latter states. We also indicated and discussed the conjugate fields and susceptibilities associated with these hypertoroidal moments, and the coupling between these moments and the strain. We further pointed out various important differences related to hypertoroidal moment, such as the facts that (i) the magnetic hypertoroidal moment is an axial vector while the electric hypertoroidal moment is a polar vector; (ii) the hysteresis hypertoroidal moment-versus-applied field occurs in an opposite fashion in an hysteron made of a ferroelectric with respect to an hysteron made of a ferromagnet; and (iii) the hypertoroidal moment can have different possible values in a periodic system while it is uniquely defined in a zero-dimensional material.

It may also be interesting in the future to determine if other order parameters need to be defined in order to characterize states with increasing complexity. For instance, one may wonder if there are dipolar structures for which the sole order parameter involves a *triple* cross product of the local dipoles with the vectors locating their positions.

Acknowledgements We hope that this article will be of benefits to scientists interested in complex dipolar states, and acknowledge support from ONR grants N00014-04-1-0413 and N00014-08-1-0915, NSF grants DMR-0701558, DMR-0404335, and DMR-0080054 (C-SPIN) and DOE grant DE-FG02-05ER46188. Some computations were made possible thanks to the MRI Grants 0421099 and 0722625 from NSF. S.P. also appreciates the support of grants RFBR-07-02-00099&08-02-92006NNS.

References

1. Dubovik VM, Tugushev VV (1990) Phys Rep 187:145
2. Naumov I, Bellaiche L, Fu H (2004) Nature 432:737
3. Bader SD (2006) Rev Mod Phys 78:1
4. Prosandeev S, Bellaiche L (2008) Phys Rev B 77:060101 (R)
5. Prosandeev S, Bellaiche L (2008) Phys Rev Lett 101:097203
6. Dubovik VM, Cheshkov AA (1975) Sov J Part Nucl 5:318
7. Ascher E (1975) In: Freeman A, Schmidt H (eds) Magnetoelectric interaction phenomena in crystals. New York
8. Malashevich A, Vanderbilt D (2008) Phys Rev Lett 101:037210
9. Dzyaloshinskii I (1958) J Phys Chem Solids 4:241
10. Moriya T (1960) Phys Rev 120:91
11. Dubovik VM, Martsenyuk MA, Saha B (2000) Phys Rev E 61:7087
12. Callen HB, Welton TA (1951) Phys Rev 83:34
13. Resta R (1994) Rev Mod Phys 66:899
14. Chien CL, Zhu FQ, Zhu J-G (2007) Phys Today 92:40
15. Prosandeev S, Ponomareva I, Kornev I, Bellaiche L (2008) Phys Rev Lett 100:047201
16. Hoffmann H, Steinbauera F (2002) J Appl Phys 92:5463
17. Antropov VP, Tretyakov SV, Harmon BN (1997) J Appl Phys 81:3961
18. Vedmedenko EY, Ghazali A, Levy J-CS (1998) Surf Sci 391:402
19. Cowburn RP, Koltsov DK, Adeyeye AO, Welland ME, Tricker DM (1999) Phys Rev Lett 83:1042
20. Shinjo T, Okuno T, Hassdorf R, Shigeto K, Ono T (2000) Science 289:930
21. Zhong W, Vanderbilt D, Rabe KM (1995) Phys Rev Lett 73:1861
22. Zhong W, Vanderbilt D, Rabe KM (1994) Phys Rev B 52:6301
23. Bellaiche L, Garcìa A, Vanderbilt D (2002) Phys Rev Lett 84:5427
24. Bellaiche L, Garcìa A, Vanderbilt D (2002) Ferroelectrics 266:41
25. Naumov II, Fu H (2005) cond-mat/0505497
26. Ponomareva I, Naumov II, Kornev I, Huaxiang F, Bellaiche L (2005) Phys Rev B 72:140102(R)
27. Ponomareva I, Naumov II, Bellaiche L (2005) Phys Rev B 72:214118 (2005)
28. Fu H, Bellaiche L (2003) Phys Rev Lett 91:257601

29. Almahmoud E, Navtsenya Y, Kornev I, Fu H, Bellaiche L (2004) Phys Rev B 70:220102(R)
30. Metropolis N, Rosenbluth AW, Rosenbluth MN, Teller AH, Teller E (1953) J Chem 21:1087
31. Alder BJ, Wainwright TE (1959) J Chem Phys 31:459
32. Rothman J, Kläui M, Lopez-Diaz L, Vaz CAF, Bleloch A, Bland JAC, Cui Z, Speaks R (2001) Phys Rev Lett 86:1098
33. Zhu FQ, Chern GW, Tchernyshyov O, Zhu XC, Zhu JG, Chien CL (2006) Phys Rev Lett 96:027205
34. Huber M, Zweck J, Weiss D (2008) Phys Rev B 77:054407
35. Arrott AS (2003) J Magn Magn Mater 258–259:25
36. Buchanan KS, Roy PE, Fradin FY, Guslienko KYu, Grimsditch M, Bader SD, Novosad V (2006) J Appl Phys 99:08C707
37. Okuno T, Mibu K, Shinjo T (2004) J Appl Phys 95:3612
38. Giesen F, Podbielski J, Botters B, Grundler D (2007) Phys Rev B 75:184428
39. Hubert A, Schafer R (1998) Magnetic domains: the analysis of magnetic microstructures. Springer, Berlin
40. Schabes ME, Bertram HN (1988) J Appl Phys 64:1347
41. Prosandeev S, Bellaiche L (2007) Phys Rev B 75:094102
42. Prosandeev S, Kornev I, Bellaiche L (2007) Phys Rev B 76:012101
43. Lai B-K, Ponomareva I, Naumov V, Kornev I, Huaxiang Fu, Bellaiche L, Salamo GJ (2006) Phys Rev Lett 96:137602
44. Kornev I, Fu H, Bellaiche L (2004) Phys Rev Lett 93:196104
45. Streiffer SK, Eastman JA, Fong DD, Thompson C, Munkholm A, Ramana Murty MV, Auciello O, Bai GR, Stephenson GB (2002) Phys Rev Lett 89:067601
46. Landau L, Lifshitz E (1935) Phys Z Sowjetunion 8:153
47. King-Smith RD, Vanderbilt D (1993) Phys Rev B 47:1651
48. Ederer C, Spaldin NA (2007) Phys Rev B 76:214404
49. Vanderbilt D, King-Smith RD (1993) Phys Rev B 48:4442
50. Resta R (1994) Rev Mod Phys 66:899